Linker-Induced Anomalous Emission of Organic-Molecule Conjugated Metal-Oxide Nanoparticles

Volodymyr Turkowski,[†,‡] Suresh Babu,[#] Duy Le,[†] Amit Kumar,[§] Manas K. Haldar,[▽] Anil V. Wagh,[▽] Zhongjian Hu,[†] Ajay S. Karakoti,[○] Andre J. Gesquiere,[†,⊥,¶] Benedict Law,[▽] Sanku Mallik,[▽] Talat S. Rahman,[†,‡] Michael N. Leuenberger,[†,‡] and Sudipta Seal[‡,§,*]

[†]Department of Physics, [‡]NanoScience Technology Center, [§]Advanced Materials Processing and Analysis Center, Mechanical Materials Aerospace Eng, [⊥]Department of Chemistry, and [¶]College of Optics and Photonics, University of Central Florida, Orlando, Florida 32816, United States, [#]Centre for NanoScience and Technology, Madanjeet School of Green Energy Technologies, Pondicherry University, Pondicherry-605 014, India, [▽]Department of Pharmaceutical Sciences, North Dakota State University, Fargo, North Dakota, United States, and [○]Environmental and Molecular Sciences Laboratory, Pacific Northwest National Laboratory, Richland, Washington 99354, United States

ABSTRACT Semiconductor nanoparticles conjugated with organic- and dye-molecules to yield high efficiency visible photoluminescence (PL) hold great potential for many future technological applications. We show that folic acid (FA)-conjugated to nanosize TiO_2 and CeO_2 particles demonstrates a dramatic increase of photoemission intensity at wavelengths between 500 and 700 nm when derivatized using aminopropyl trimethoxysilane (APTMS) as spacer-linker molecules between the metal oxide and FA. Using density-functional theory (DFT) and time-dependent DFT calculations we demonstrate that the strong increase of the PL can be explained by electronic transitions between the titania surface oxygen vacancy (OV) states and the low-energy excited states of the FA/APTMS molecule anchored onto the surface oxygen bridge sites in close proximity to the OVs. We suggest this scenario to be a universal feature for a wide class of metal oxide nanoparticles, including nanoceria, possessing a similar band gap (~3 eV) and with a large surface-vacancy-related density of electronic states. We demonstrate that the molecule–nanoparticle linker can play a crucial role in tuning the electronic and optical properties of nanosystems by bringing optically active parts of the molecule and of the surface close to each other.

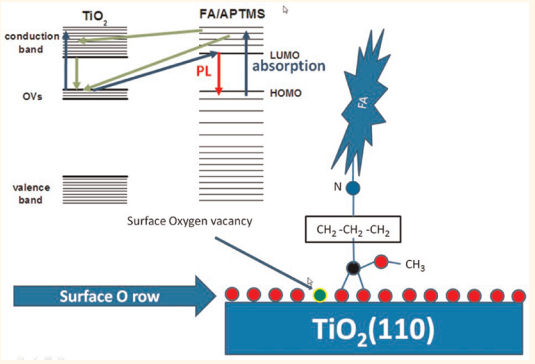

KEYWORDS: photoluminescence · semiconductor nanostructures · organic-molecule conjugated nanoparticles · linker molecules

The interactions of the surface of nanomaterials with high quantum-absorption efficient dye molecules are useful in chemical and physical sensing applications and form the basis for molecular photoelectronic devices. Small highest occupied molecular orbital–lowest unoccupied molecular orbital (HOMO–LUMO) gap (in the visible range) and charge/electron transfer properties of different organic and dye molecules are often used in designing modern photovoltaic devices such as dye sensitized solar cells (DSSCs).[1] In fact, such molecules attached to semiconductor (nano-) structures can also result in a strong increase in visible light photoabsorption. The inverse process of photoabsorption, photoluminescence (PL), also provides a wide area of applications, from organic solar concentrators to fluorescence tags in nanomedicine.[2] For instance, in solar concentrators the absorbed solar energy is re-emitted and transported through waveguides from the original place of absorption to avoid the use of focused mirrors.[3] In therapeutic applications of nanoparticles, the strong PL of organic-(dye-)molecule/nanoparticle systems is used to detect different malignant tumors.[4] Such a combination of nanoparticles and dye molecules offers great promise in chemical[5] and biological[6] sensing applications, and especially in fluorescent labeling.[7]

To covalently bind the nanoparticles to organic molecules (such as fluorescent tags, biomolecules, antibodies, and receptors) various molecular linkers are often used. In particular such silanes as the APTMS molecule can be used very effectively for this purpose.[8–13] Having a large HOMO–LUMO gap (~4.4 eV),[13] APTMS is not optically active by itself.

Interestingly, our experiments show that the covalent linking (according to Scheme 1) of a folic acid (FA)/APTMS molecule to either titanium oxide (TiO_2) or cerium oxide (CeO_2) nanoparticles (5–10 nm in diameter) results

* Address correspondence to Sudipta.Seal@ucf.edu.

Received for review January 12, 2012 and accepted May 5, 2012.

Published online May 05, 2012
10.1021/nn301316j

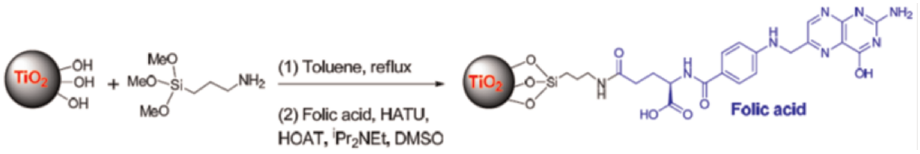

Scheme 1. Surface functionalization of TiO_2 nanoparticles.

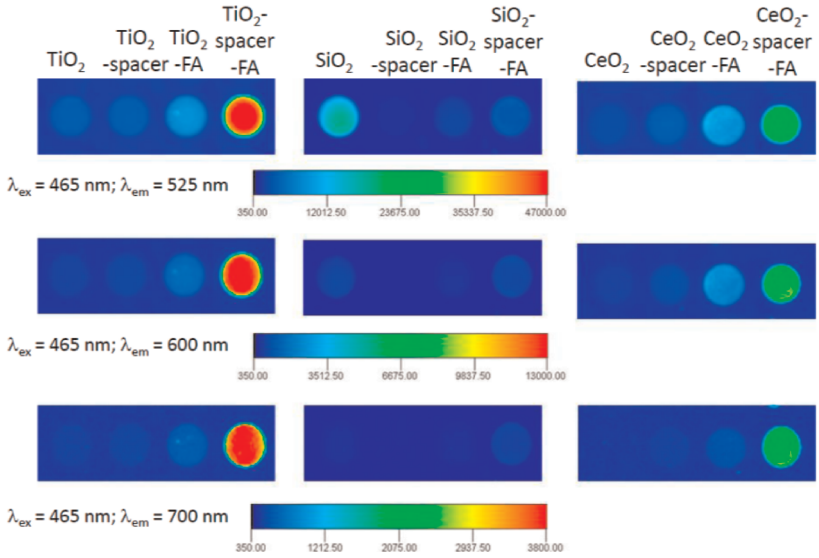

Figure 1. In-suspension images of NP, NP−APTMS, NP-FA, NP−APTMS/FA (NP = TiO_2, CeO_2, SiO_2) under 465 nm excitation at different emission wavelengths of 525, 600, and 700 nm. Various permutations and combinations show that nanoceria or nanotitania linked to FA with the spacer shows bright fluorescence, in contrast to nanosilica, which does not show any fluorescence upon linking with spacer and FA. It was clearly observed that only FA/APTMS-functionalized nanoceria and nanotitania show bright fluorescence, whereas direct linking of nanoparticles with APTMS alone or with FA alone do not lead to any significant observed fluorescence. Taken together, these observations emphasize the importance of covalent linking of both the APTMS linker (spacer) and FA units to the ceria and titania nanoparticles.

in a strong visible PL of the APTMS/FA-nanoparticle system under 465 nm excitation (Figure 1). Such an increase in PL is central to the particles of nanoscale dimensions since this was not observed for covalently linked micrometer-sized particles. Treating TiO_2 nanoparticles as a prototype support, we demonstrate that this enhancement in PL is due to a combined effect of a decrease in the HOMO−LUMO gap of FA caused by covalent linking with APTMS and the direct involvement of TiO_2 surface OV states. This conclusion is supported by our analysis of the possible mechanisms of electron transfer between the covalently linked molecules and the nanoparticle surface, and estimation of the characteristic time scales for the optical response of the TiO_2−APTMS/FA nanosystem (from electron excitation and electron−hole recombination). The role of surface states and band gap is further corroborated by our results in examining two other systems, nanoparticles of CeO_2 (with a band gap close to that of TiO_2) and silicon dioxide (SiO_2) (with a band gap higher than that of TiO_2). Despite the fact that the idea of linking nanoparticles and dye molecules through a ligand is well-known, in particular for enabling Graetzel cell,[14] and it is actively used in different areas of nanotechnologies (see also refs 15 and 16, where the linker was responsible for alignment of the nanoparticle and molecule energy levels), to our knowledge this is the first demonstration that the interaction of surface defect states of nanoparticles with organic molecules, brought close by a linker, leads to a strong enhancement of PL.

RESULTS

The fluorescence imaging of bare and folic-acid functionalized nanoparticles (<10 nm in size) using APTMS (labeled as spacer) is depicted in Figure 1. The nanoparticles were imaged by exciting the well-dispersed suspension at 465 nm, and the images were collected at emission wavelengths of 525, 600, and 700 nm. A comparison of the observed fluorescence from bare TiO_2 and various controls such as TiO_2−APTMS, TiO_2−FA, and TiO_2−APTMS/FA shows that high-fluorescence intensity is observed only when TiO_2 is covalently linked to FA using APTMS as a linker (spacer) molecule. A very weak fluorescence is observed for nonconjugated nanoparticles and FA. Nor does direct conjugation of APTMS with FA or conjugation of nanoparticles with only FA improve the fluorescence properties of the metal−oxide nanoparticles. In comparison to TiO_2, SiO_2 nanoparticles functionalized under the same protocol does not show such an

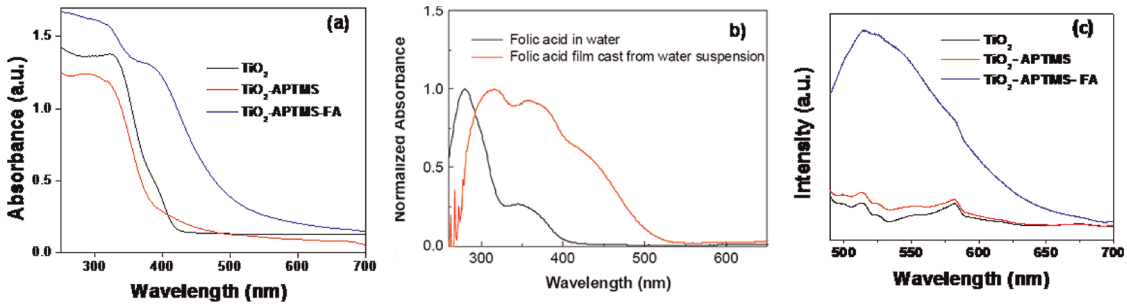

Figure 2. Optical absorption spectra for TiO_2, TiO_2—APTMS, TiO_2—APTMS/FA, and FA systems. (a) The case of TiO_2, TiO_2—APTMS, and TiO_2—APTMS/FA. A marginal blue shift from 415 to 385 nm (3 to 3.22 eV) was observed upon attaching APTMS but a red shift to 490 nm (2.5 eV) resulted upon conjugating with APTMS/FA. (b) UV—vis absorption spectrum of FA in water and corresponding UV—vis absorption spectrum of a FA film cast from the solution in water. A significant broadening and red-shift of the absorption spectrum can be observed. (c) PL spectra (excitation at 465 nm) for TiO_2, TiO_2—APTMS, and TiO_2—APTMS/FA show broad fluorescence only from functionalized TiO_2 nanoparticles.

increase in fluorescence intensity (Figure 1b), whereas CeO_2 nanoparticles show a much greater increase in fluorescence intensity after functionalization. The observed fluorescence of TiO_2 and CeO_2 nanoparticles conjugated with APTMS/FA over a broad range of wavelengths suggests that the nanoparticle system can emit over a range of wavelengths from a single excitation wavelength. A comparison of the intensities reveals that the TiO_2—APTMS/FA nanoparticles display the highest intensity, followed by those of CeO_2—APTMS/FA, while (interestingly) SiO_2—APTMS/FA nanoparticles were barely fluorescent (Figure 1). Thus it is evident that for strong emission to occur, the band gap of the metal oxide nanoparticles is a critical factor. Nano-CeO_2 and nano-TiO_2 (with a band gap in the range of 3.0—3.2 eV) fulfill all requirements for the highly fluorescent composite system. It was shown previously that photoelectrodes composed of only FA/TiO_2 hybrid material which can generate a photocurrent in the 300—600 nm window,[17] can be used in optoelectronic switches. However, the same study showed that direct linking of FA to TiO_2 did not display significantly visible PL. For the harvesting and transportation of solar energy it would be extremely useful to modify these materials, however, in such a way as to produce a significant PL as well. In the present work, we find that by selectively alignment of the electronic states of the participating molecules and nanoparticles linker molecules can lead to a strong increase (about 5 times) in the visible PL over that of the hybrid nanoparticle—FA system. We identify two critical requirements for designing such a composite nanoparticle system: (a) relative broadness of band gap and (b) presence of surface states (or oxygen vacancies [OVs]). It must be noted that mere physical mixing of the nanoparticle, linker, and FA does not lead to any increase in fluorescence (data not shown). It is only when the molecules are linked covalently that there is an enhancement in the PL signal, since covalent linking causes the electronic fields of the participating molecular orbitals to overlap and be perturbed. The covalent linking of the molecules to the nanoparticles under consideration (CeO_2, TiO_2, and SiO_2) was confirmed using Fourier transform infrared (FTIR) spectroscopy as well as X-ray photoelectron spectroscopy (XPS) (Supporting Information, Figures SI-1 and SI-2). Furthermore, results from high resolution transmission electron microscopy (HRTEM) verify that the size of the nanoparticles remains unaltered after their surface modification (see SI-3 for TiO_2 as an example). We further evaluated the changes in the absorption and emission properties of nanoparticles upon surface modification. Optical absorption spectra of bare TiO_2 nanoparticles as well as APTMS- and APTMS/FA-conjugated TiO_2 nanoparticles are shown in Figure 2a. The attachment of APTMS to TiO_2 resulted in a blue shift in the absorption edge to 385 nm (3.22 eV) and the attachment of FA to TiO_2—APTMS resulted in a broad spectrum with a red shift in the absorption edge to 490 nm (2.5 eV). The observed red shift can most likely be ascribed to the aggregation of FA molecules on the surface of the metal-oxide nanoparticles, leading to a red shift in the absorption of FA. The red-shift and broadening of the FA absorption spectrum into the visible region was confirmed by preparation of FA films, as shown in Figure 2b. The corresponding photoluminescence spectra of TiO_2, TiO_2—APTMS, and TiO_2—APTMS/FA are shown in Figure 2c. Upon excitation at 465 nm neither pure TiO_2 nor TiO_2 conjugated with APTMS showed any characteristic emission, but the TiO_2—APTMS/FA system exhibited a broad band centered at 525 nm.

It is important to note that a red shift in the optical absorption of nanoparticles was previously observed in $TiO_{2-x}N_x$ sputtered films as a result of nitrogen substitution in the lattice.[18] Moreover, an increase in the visible PL of the system was reported as well.[19] The TiO_2—APTMS/FA system considered herein is different and has several advantages over the one with doping. Besides the fact that in our samples the surface modification of nanoparticles with linker and organic molecules leads to higher PL, our technique does not rely

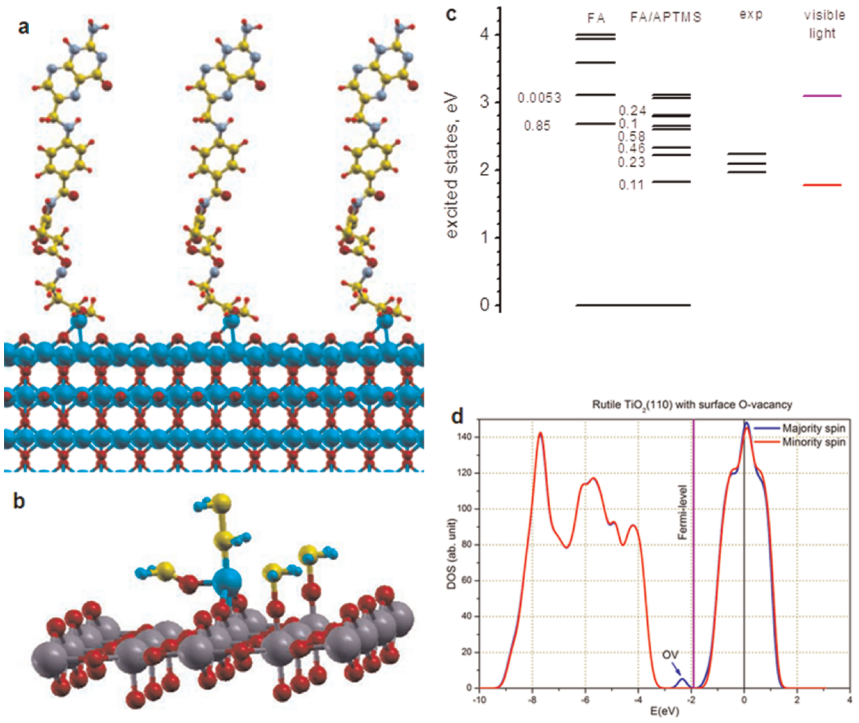

Figure 3. Numerical analysis of the properties of TiO_2(110)−APTMS/FA system. (a) The model structure of the APTMS/FA molecules coupled to the TiO_2(110) surface. (b) The structure of the TiO_2(110) surface together with the details of the coupling of trimethoxylane molecules to the surface.[9] Two $-OCH_3$ groups on the right are attached to the surface titanium atoms, and the remaining part of the APTMS molecule is coupled to two oxygen bridge atoms. (c) The excitation energy levels of the FA and APTMS/FA systems (with corresponding dipole moments). The experimental PL peaks and the visible light range are also shown. (d) Calculated density of states of the TiO_2 nanoparticle with the (110) surface and the occupied OV states lie approximately 0.7 eV below the conduction band.

on doping, which may affect the crystalline properties of material by modifying the bulk lattice structure (substitutional or interstitial doping), making the system less controllable for further applications. Also, doping is not feasible to the same extent for many materials. In contrast, material-surface modification of the type obtained here is, in principle, suitable for all materials for which proper surface states and band gaps are present. The strategy proposed here is thus universal and offers the prospect of eventually enabling the manipulation of molecular levels in electronics.

In addition, the use of biomolecules such as folic acid as an alternative to dye molecules has several advantages from the biotechnical point of view. The TiO_2−APTMS/FA conjugated system can be used for more efficient light harvesting and (coherent) charge transfer, in which the APTMS/FA molecule serves as the light-harvesting part, and TiO_2 as the charge separator. Lastly, the anchoring groups on the APTMS and FA can be chemically linked to the surface of various nanoparticles.

It has been reported that the surface OV states can lead to a small PL at $\lambda = 505$ nm at temperatures below (approximately) 600 K even in the case of bare unconjugated TiO_2 nanoparticles[20] irradiated with $\lambda =$ 325 nm photons. Since this effect disappeared as the temperature was increased, it was suggested that TiO_2 nanoparticles form the anatase structure with many OV states at low temperatures, and the rutile structure at higher temperatures, with few such states. However, as calculations, including the present ones, demonstrate,[21,22] the oxygen vacancy states are occupied, that is, they lie below the Fermi level, so that excitations from the valence band to these states are forbidden. In addition, since in the current study the external light source has wavelength $\lambda = 465$ nm, the attendant energy (~2.7 eV) cannot lead to any absorption of light by the bare unconjugated nanoparticles.

DISCUSSION

Model of the Photoluminescense Mechanism. To understand the effect of linking of APTMS and FA on the electronic/fluorescence properties of FA, the optimized structures of the FA and APTMS molecules as well as of the coupled APTMS/FA system were calculated by DFT using the Gaussian 03 code[23] with the B3LYP exchange correlation-potential[24−26] (see also Supporting Information, section SI-4). The results are presented in Figures 3a, 3b and Figures SI-5, SI-6.2, which show that the geometrical structure of the molecules does not change much after the coupling (For the structural and electronic properties of FA and APTMS, see refs 13, 17, and 27). However, the coupling

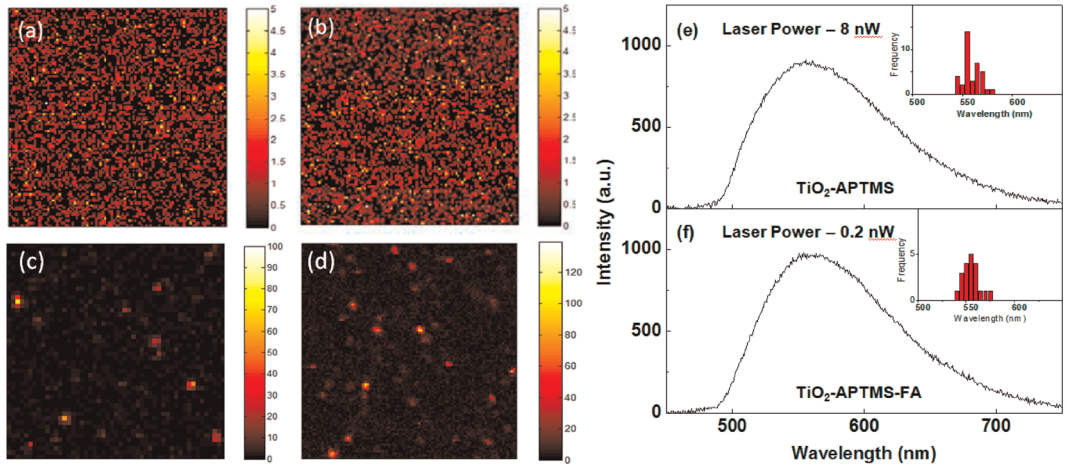

Figure 4. Confocal fluorescence images under 488 nm laser excitation of (a) TiO_2 nanoparticles (excitation power, 6 W/cm^2; scan range, 20 × 20 μm^2); (b) APTMS (excitation power, 6 W/cm^2; scan range, 30 × 30 μm^2); (c) TiO_2–APTMS nanoparticles (excitation power, 6 W/cm^2; scan range, 10 × 10 μm^2) and (d) TiO_2–APTMS/FA nanoparticles (excitation power, 0.15 W/cm^2; scan range, 10 × 10 μm^2). Fluorescence intensity is represented as counts/dwell (5 ms). To obtain a similar count rate for TiO_2–APTMS/FA nanoparticles as compared to TiO_2–APTMS nanoparticles the excitation power had to be lowered by a factor of 40, illustrating the significant enhancement of TiO_2 emission in the presence of FA. SPS ensemble spectra of (e) TiO_2–APTMS nanoparticles under 8 nW excitation and (f) TiO_2–APTMS/FA nanoparticles under 0.2 nW excitation. The inset presents the emission peak wavelength distribution histogram.

does lead to a significant change in the position of the energy levels of the molecules. This is further verified by our calculations based on TDDFT, which show that the presence of the APTMS molecule leads to a decrease of the HOMO–LUMO gap of the FA system (Figure 3c), so that a larger part of the visible spectrum can be absorbed. Particularly, we find absorption at λ = 465 nm (the absorption of pure FA is very low at wavelengths above λ = 360 nm). The acceptor part of the FA is on top of the molecule (the LUMO excitation), but as shown in ref 15 some of the molecular orbitals for higher excited states occupy the lower part of the FA, making the charge transfer between the adsorbed molecules and the nanoparticles possible. In principle, packing of the FA molecules into a molecular crystal could have led to absorption at λ = 450 nm (for details, see for example, ref 17), resulting in some (rather weak) visible PL. Our experiments in solution indicate a red shift in the TiO_2–APTMS/FA sample, which could arise from the molecular packing of FA as well. However, the absorption of free FA in solution suggests that molecular packing is absent in solution and may occur only upon drying the samples as films (Figure 2b). Thus the absorption of TiO_2–APTMS/FA in the visible region cannot be ascribed solely to the molecular packing, as we have observed the absorption and emission from aqueous suspension of TiO_2–APTMS/FA samples (Figures 1a and 2a).

The in-solution data as shown in Figure 1 depict the fluorescence properties of the conjugated system in suspension. To further evaluate the properties of the TiO_2–APTMS/FA system and exclude the effects of solvent, nanoparticle precipitation and aggregation nanoparticles were studied on an individual basis in the solid state through single particle spectroscopy (SPS). As shown in Figure 4a,b, samples of TiO_2 nanoparticles or APTMS drop-cast directly on cover glass slides do not show any fluorescence signal under an excitation power of 6 W/cm^2. No emission was observed even under 10-fold higher excitation power for either sample (data not shown). In contrast, when APTMS was chemically linked to TiO_2 nanoparticles, the resulting TiO_2–APTMS nanoparticles exhibited a detectable photoluminescence under 6 W/cm$_2$ excitation power (Figure 4c). That the corresponding SPS ensemble spectrum of the TiO_2–APTMS conjugate in Figure 4e shows an emission maximum at λ = 555 nm can be attributed to radiative recombination of TiO_2 self-trapped states.[28] When FA is conjugated with TiO_2–APTMS nanoparticles, the photoluminescence signal is again strongly enhanced. To obtain an emission intensity for the TiO_2–APTMS/FA nanoparticles that is similar to the case of the TiO_2–APTMS nanoparticles, the excitation power had to be lowered by a factor of 40, illustrating the significant enhancement of TiO_2 emission in the presence of APTMS/FA (Figure 4d, f). The relatively weak emission in the TiO_2–APTMS case can be explained by a mechanism related to the surface OV states, as in the TiO_2 case.[29]

The absence of any significant visible light PL (not shown) for commercial microparticles (size ≈ 1000 nm) conjugated to APTMS/FA suggests that the surface of the nanoparticles plays an important role (since in the 5–10 nm particles the number of surface and bulk atoms is comparable). The changes in emission characteristics of the nanoparticle-conjugated APTMS/FA system can be further understood from the results of DFT calculations. We considered a representative case

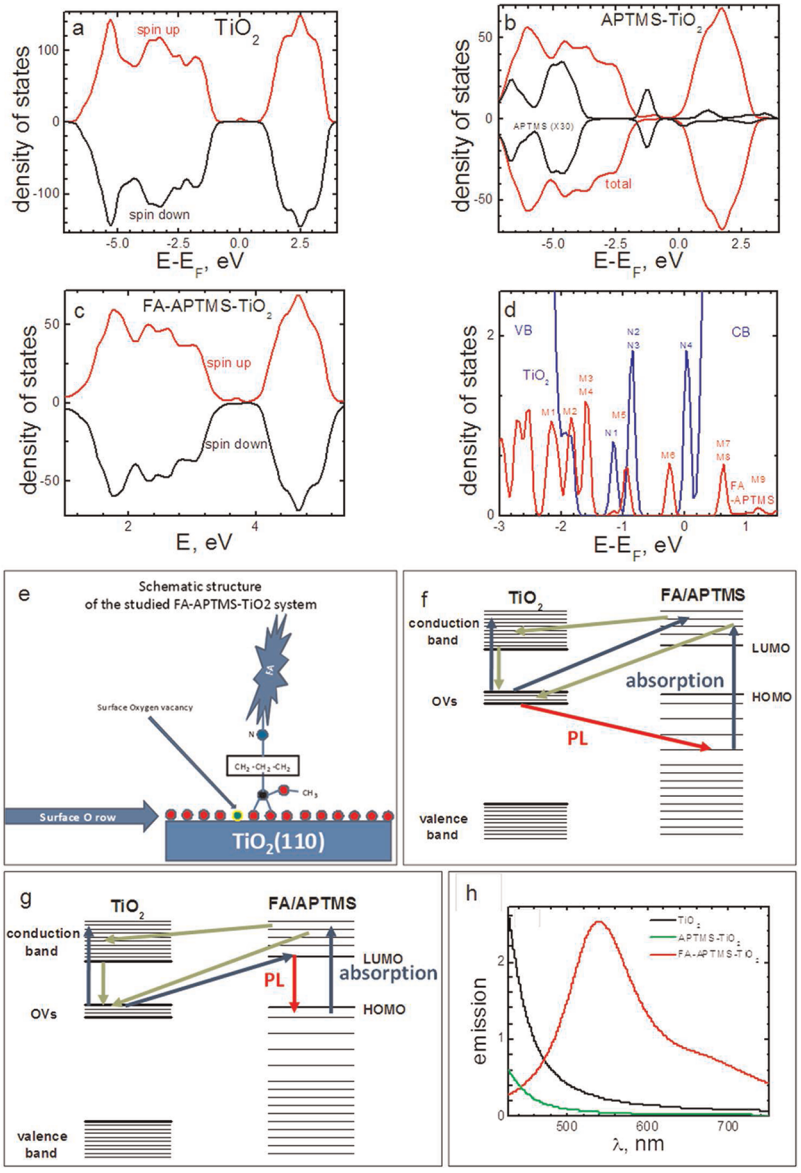

Figure 5. Theoretical analysis of the optical properties of the TiO_2—APTMS/FA system. (a) Density of states of the TiO_2 nanoparticle as a function of energy for the spin up (red) and spin down (black) states. The Fermi energy corresponds to E = 0 eV. The small peak just below the Fermi energy corresponds to the OV states. (b) The total (red) and APTMS subsystem (black) density of states of the TiO_2—APTMS system. The APTMS density of states is multiplied by 30. The curves with positive and negative values are the spin up and spin down densities of states, correspondingly. (c) The density of states of TiO_2—APTMS/FA. The notations are the same as in panel a. (d) The partial densities of states of spin-up electrons of APTMS/FA (red) and TiO_2 (blue) of the TiO_2—APTMS/FA system in the optically active region. VB and CB stand for the valence and conduction bands, correspondingly. M1—M9 correspond to the molecular levels and N1—N4 to the TiO_2 states inside the gap, while N1—N3 correspond to the OV states. (e) Coupling between the APTMS/FA and TiO_2(110) subsystems shows that the lowest energy coupled configuration of TiO_2(110) surface and trimethoxylane molecules corresponds to the case in which the silane group (the bottom of the APTMS molecule in our case) is attached to the raw oxygen bridge of the (110) surface by a two oxygen coupling. (f—g) The schematic mechanisms of the main processes which lead to the PL of TiO_2—APTMS/FA system. The TiO_2 and the molecule states are on the left and right, correspondingly. The Fermi level is right above the OV band. The blue, red, and green arrows correspond to the absorption, PL, and nonradiative (weakly radiative) processes. (f) A photon absorbed by the molecule (right blue) creates an excited electron above the LUMO and a hole below the HOMO states. The hole recombines with OV electron owing to the vicinity of both states, leading to the PL (red). The excited electron on the molecule electron fills the empty OV state (green). The injection of electrons from the highly excited FA—APTMS states to the conduction band of TiO_2 is also rather efficient since FA, which contains a large part of the lowest excited state (larger than HOMO energy) charge, is a good charge donor (see, *e.g.*, ref 17). (g) As a result of the photon absorption, the molecular HOMO electron moves to an excited state with the energy higher than that of the LUMO (right blue) and an OV electron moves to the molecular LUMO state (middle blue). The LUMO—HOMO de-excitation process leads to the PL (red). Similarly to the previous case, the remaining excited on the molecule electron fills the empty OV state (right green). As our calculations show, the last mechanism can be considered as the dominant one. (h) The theoretical results for the emission spectrum of the TiO_2, TiO_2—APTMS, and TiO_2—APTMS/FA system (arbitrary units).

of the rutile TiO_2 nanoparticle with the lowest energy (110) surface[8] coupled to the APTMS/FA molecules. Note that the case of anatase TiO_2 should be similar, since in anatase the lowest-energy surface (TiO_2 (101)) has oxygen bridges, and the lowest-energy surface OV states present on the bridges. Calculations demonstrate that the OVs may tend to occupy a subsurface layer (with energy lower than that of the surface bridge sites[30]). However, these states are also pretty close to the oxygen bridges where APTMS anchors have to be attached.

In both free TiO_2 and molecular-conjugated-TiO_2 with and without the APTMS linker, we find that the nanoparticle Fermi level is above the OV band (relatively small red-curve peaks on red right below 0.0 eV in Figure 5a,b, and right below the Fermi energy at 4 eV in Figure 3c, see also Figure 3d, where the OV DOS is shown), indicating that these states are occupied. This explains the absence of the TiO_2 absorption at $\lambda = 465$ nm. The OVs occupy the oxygen bridge rows on the surface (Figure 5e). As shown in Figure 5e, the OVs are close to the molecular two-oxygen bonds coupled to the surface; however since the OV band electron wave function is spread over several bridging oxygen atoms (Supporting Information, Figure SI-6.2), the vacancies should not necessarily be too close to APTMS. The correlation effects were included to obtain the OV band in accordance with previous reports.[31] The calculations of the band structure of the TiO_2 five-layer slab were performed using the VASP4.6 code (ref 17 in SI) (also see SI) with the GGA+U exchange correlation potential. We find that the OV states and their vicinity to the APTMS/FA states are crucial for explaining the PL of the TiO_2−APTM/FA system.

A scheme of the coupling of the APTMS/FA structure to the TiO_2 (110) surface is presented in Figure 5e. Consistent with ref 9, the lowest energy coupled configuration of the TiO_2(110) surface and trimethoxysilane molecules corresponds to the case where the silane group (the bottom of the APTMS molecule in our case) is attached to the oxygen bridge row of the (110) surface through two-oxygen coupling.

After the coupling, one of the three OCH_3 groups remains on the molecule, while the other two are detached and bind to the surface Ti sites. Since the OVs and the APTMS oxygen atoms, which bind to the surface, are on the same oxygen-bridge rows, the vicinity enables excitation of these electrons to the molecular states and also facilitates trapping of the OV electrons by the APTMS/FA holes. Such processes do not take place in cases in which the molecule is attached to atoms far from the bridges (in TiO_2/FA, for example, FA is attached to a titanium atom). The density of states of the coupled system presented in Figure 5c,d suggests the following channels by which the excited system might generate the PL:

(1) The APTMS/FA molecule absorbs the light by exciting electrons to state M7 and above and leaving holes behind in the M1−M6 states. Recombination of these holes with the OV band electrons (states N1−N3) leads to the PL. The excited electrons on the molecules (states M7 and above) refill the empty OV band states through nonradiative or weak, nonvisible radiative processes.

(2) The OV electrons are excited to the APTMS/FA LUMO state. They recombine with the HOMO holes of the APTMS/FA molecule excited to higher states, leading to a strong emission. The other excited electrons on the APTMS/FA molecule refill the empty OV states irradiatively or with some possible weak infrared emission. It is important to note that for this specific mechanism the 465 nm (2.7 eV) source cannot excite the APTMS/FA electrons from the HOMO to the LUMO state (2.3 eV); the role of the OV states is thus critical. A very large dipole moment of the OV to APTMS/FA LUMO transition (∼0.58) also favors this particular mechanism. Additionally, in agreement with ref 11, the absorption and emission spectra of FA are rather different from the ones observed in the APTMS/FA-conjugated TiO_2 nanoparticles, suggesting again that the surface states of TiO_2 nanoparticles play a very important role.

Since the lifetime of the holes on the APTMS/FA levels (M1−M5) below the molecular HOMO state (M6) considered in case (1) is much shorter than the lifetime of the holes in the molecular HOMO state (M6), mechanism (2) has to be considered as the dominant one. It is important to note that the latter value for the molecular excited lifetime of NP−APTMS/FA is significantly larger than the experimental result for the folic acid molecule (∼10 ns, see refs 32 and 33). This can be explained by an increase of the spatial separation between the charge distribution for the molecular HOMO and LUMO states due to the APTMS molecule. The schematic PL mechanisms are presented in Figure 5f−g. Theoretically calculated PL of the TiO_2, TiO_2−APTMS, and TiO_2−APTMS/FA is presented in Figure 5h, obtained using the formula below.

$$I_{\mathrm{Lum}}(q) \approx \frac{\pi\hbar}{\varepsilon_0 V} \sum_{l,m} \frac{\omega(q)|d_{lm}|^2\Gamma}{(E_l - E_m - \omega(q))^2 + \Gamma^2}$$

where V is volume of the system, $w(q)$ is the photon spectrum, E_l and E_m are the energy levels, d_{lm} is the corresponding dipole moment, and Γ is the level broadening (see, *e.g.,* ref 34). This equation is valid at moderate temperatures and minimal perturbation from external fields. Clearly, our calculations agree with the experimental data (Figure 2c and Figure 4f) reasonably well. In particular, given a large molecular coverage, the TiO_2−APTMS spectrum is shifted to higher energies with respect to that of bare TiO_2. Our calculations show that the OV state extends rather far inside the APTMS molecule (Supporting Information, Figure

SI-6.2) which makes the OV to APTMS/FA excitations and the electron−hole recombination favorable. Since the FA molecule couples to Ti sites through two oxygen atoms (bottom part of the FA, Figure SI-5) without any linker molecule, the FA holes are far from both the surface oxygen bridges and the OV electron states of titania, resulting in decreasing the probability of electron−hole recombination and consequently a reduced PL. Analysis of the dipole moments for the states in Figure 5d, shows that the external source with energies 2.4−2.8 eV (443−517 nm) will lead to a PL at 2−2.3 eV (539−620 nm), while there will be no PL if the external source energy is below 2 eV (above 620 nm). It is important to note that in the calculation of the PL spectrum, the GGA results for the energy levels (TiO_2 bandwidth and the APTMS/FA HOMO−LUMO gap) presented in Figure 5d were corrected (by using the experimental values of 3 and 2.3 eV, correspondingly), since DFT calculations underestimate the value of the band gap (more details on the PL mechanism calculations can be found in SI-6.1).

The estimated times τ for the electron excitation and electron−hole recombination processes for the transitions between states *l* and *m* can be obtained by using for τ (in atomic units):

$$\tau \approx \frac{c^3}{2(E_l - E_m)^2 f_{lm}}$$

where *c* is speed of light and f_{lm} is the corresponding oscillator strength.[32] In particular, for the main processes that lead to the PL (Figure 5g) we obtained estimated values ∼41 ns for the PL process transition (red arrow) and an order of magnitude longer time for the absorption transition processes (middle and right blue arrows). Our estimation of quantum yield gives an approximate value of 86%. Such a high value results from the fact that the OV and molecular excited states are close to each other, which favors the excitation transition. On the other hand, the molecular LUMO to HOMO photoluminescence transition happens with efficiency close to 100%. Some of the light is absorbed by the nanoparticle (valence to conduction band) and by the molecule (HOMO to higher excited) states, which decreases "the constructive" (OV−molecule) absorption and hence the efficiency of luminescence (see Supporting Information, section SI-7).

Our results also show that strong PL due to conjugation of APTMS/FA also takes place in the case of surface-derivatized CeO_2 nanoparticles; while such an effect is absent in the derivatized SiO_2 nanoparticles (Figure 1). We hypothesize that in the case of surface-derivatized CeO_2, the mechanism responsible for the PL is essentially the same as in the TiO_2 case. In fact, both oxides have a band gap of approximately 3 eV. Also, one can expect similar defects (like OVs and oxygen-holes centers), in these nanoparticles. In the case of silica the situation can be very different because of a much larger band gap (7−9 eV, see, *e.g.*, ref 35) and different positions of the OV states in these nanoparticles,[19,35−37] inasmuch as these are situated almost in the middle of the gap. Owing to a rather large energy gap in silica, PL due to a resonant energy transfer from an excited molecule to the nanoparticle looks also improbable. Indeed, such a PL was not observed experimentally. Thus the PL process cannot be activated by the 465 nm source in the case of surface-derivatized SiO_2.

CONCLUSION

This work demonstrates that the linkers/spacers can be effectively used to modify the optical properties of the system by bringing the optically active states of both molecule and nanoparticle subsystems closer and changing the electronic structure of the system. We believe that the mechanism proposed in this paper can be of general relevance for other metal−oxide nanoparticles with similar values of the bandgap and types of vacancies, in particular CeO_2, where the defect states play an important role.

MATERIALS AND METHODS

Synthesis of Nano-titanium Oxide and Cerium Oxide. TiO_2 nanoparticle suspensions were synthesized by the hydrolysis of titanium(IV) isopropoxide (Sigma Aldrich) at elevated temperature. Titanium isopropoxide (15 mL) was added dropwise to a rapidly stirred solution of water (100 mL), ethanol (100 mL), and HNO_3 (1 N, 1 mL), which was held at reflux at 840 °C and stirred for 24 h. The particles were then washed three times with DI water by centrifugation, then dried and ground by mortar and pestle. CeO_2 nanoparticles were synthesized using base hydrolysis of solution of cerium nitrate hexahydrate (Sigma Aldrich 99.999%). A 30 mL portion of 1 N ammonium hydroxide was added dropwise under constant stirring to a solution of 4 g of cerium nitrate hexahydrate in 500 mL of water. The stirring was continued overnight, and the final pH of the solution was adjusted to 10.0 using 1 N ammonium hydroxide. The precipitate was so obtained, then dried at 100 °C in a vacuum oven. The fnal crystals were ground by a mortar and pestle and used for further testing.

Preparation of TiO_2−APTMS (Scheme 1). A suspension of TiO_2 nanoparticles (700 mg) in toluene (10 mL) was stirred with an excess of (3.5 g) 3-aminopropyltrimethoxy silane, (APTMS, NH_2-$(CH_2)_3Si(OCH_3)_3$) under refluxing conditions for 36 h. After the reaction mixture was cooled to room temperature (RT), the nanoparticles were centrifuged, washed successively with toluene (three times) and dichloromethane (2 times) and dried under vacuum, resulting in white, free-flowing nanoparticles (650 mg).

Preparation of TiO_2−APTMS/FA. TiO_2−APTMS nanoparticles (600 mg) were added to a well-stirred solution of folic acid (FA, $C_{19}H_{19}N_7O_6$, 4.49 g, 9.42 mmol) in dimethylsulfoxide (DMSO) (175 mL) at room temperature. *O*-(7-Azabenzotriazole-1-yl)-1,1,3,3 tetramethyluroniumhexafluoro-phosphate (HATU) (3.59 g, 9.42 mmol) and 1-hydroxy-7-azabenzotriazole (HOAt) (1.281 g, 9.42 mmol) were added to the flask, followed by the addition of diisopropylethylamine (DIPEA) (3.37 mL, 18.8 mmol). The reaction mixture was stirred for 36 h at RT then centrifuged, washed repeatedly with DMSO (four times), water

(two times), and acetone (two times), and dried under vacuum, resulting in light-brownish free-flowing folic-acid conjugated nanoparticles (565 mg).

CeO_2 and SiO_2 nanoparticles were functionalized following the same protocol, using the same amounts of nanoparticles and reagents.

Characterization. The size and structural characteristics of nanoparticles were investigated by X-ray diffraction (XRD-Rigaku) and transmission electron microscopy (TEM-Tecnai). To understand the functional group modifications, infrared (IR—Perkin-Elmer Spectrum One) and X-ray photoelectron spectroscopy (XPS—PHI 5400) techniques were used. The XPS studies were carried out after the binding energy was calibrated with respect to Au $4f_{7/2}$ core level at 83.9 eV. Samples were exposed to minimum radiation so as to avoid any potential damage. To understand the modifications in optical properties, optical absorption and photoluminescence spectra were investigated. The absorption studies from dry powder and from a sample suspended in water were studied using a Perkin-Elmer 750 S UV—vis NIR spectrophotometer. The photoluminescence (PL) spectra were collected from the Hitachi-7000 spectrofluorometer. Equal amounts (by weight) of powder samples were loaded in a powder cell accessory to obtain PL from each sample. The SiO_2 nanoparticles (5—15 nm BET) were purchased from Aldrich and used as received.

Confocal Fluorescence Imaging. Single-particle fluorescence images and spectra were acquired using an in-house custom built sample-scanning confocal microscope. The 488 nm line of an argon-ion laser (Melles Griot 43 series) was used as the excitation source. The laser was focused to a spot size of ~300 nm using a Zeiss 100× Fluar objective lens (NA 1.3, WD 0.17 mm). The sample was raster-scanned across the focused laser beam using a Mad City Laboratories piezoelectric stage (Nano-LP100) to create a fluorescence image of the sample. The single-particle fluorescence was detected using an avalanche photodiode (PerkinElmer SPCM-AQR-14). The single-particle fluorescence spectra were obtained by dispersing the fluorescence on a spectrograph (PI Acton SP-2156) with the grating (150 g/mm blaze, 500 nm) centered at 600 nm connected to a thermoelectrically cooled electron multiplying charge coupled device (EM-CCD, Andor iXon EM+ DU-897 BI). Each single-particle fluorescence spectrum was collected by averaging three consecutive 10 s exposures. The single-particle ensemble spectra were constructed by averaging the single-particle spectra.

Imaging of the Derivatized Nanoparticles. *In vitro* imaging was performed using the Kodak *in-Vivo* Multispectral Imaging System FX (Carestream Health, Woodbridge, CT). Briefly, well-dispersed nanoparticles (200 μL of 1 mg/mL suspension) in PBS buffer were loaded into individual wells of a clear-bottom 96-well plate (Corning, Corning, NY), which was then exposed to the excitation light source. The excitation wavelength was 465 nm. The corresponding emission wavelengths were 525, 600, and 700 nm. The exposure time was 5 min per image for four images. The images were further analyzed using computer software (Kodak Molecular imaging software, v4.5.0). All imaging experiments were conducted by suspending the particles in 50 mM phosphate containing 50 mM NaCl (pH = 8.0). Since all the experiments were performed at the same pH in the case of different systems (with and with no APTMS and others), the results clearly demonstrate strong enhancement of the intensity due to linker.

Conflict of Interest: The authors declare no competing financial interest.

Acknowledgment. The work was supported in part by DOE-DE-FG02-07ER15842 (V.T. and T.S.R.); NSF CAREER Award CBET-0746210 (A.J.G.) and through the DARPA/MTO Young Faculty Award HR0011-08-1-0059 and NSF-ECCS 072551, NSF-ECCS-0901784, AFOSR Grant No. FA9550-0910450 (M.N.L.); NIH R01 CA132034 and NSF DMR-1005011 (S.M.), NSF NIRT CBET-0708172 (S.S.), and NSF CBET-0930170 (S.S.)

Supporting Information Available: The FTIR and XPS spectra; TEM images of the nanoparticles; optimized structures of the FA and APTMS molecules: electronic charge distribution in different states of the TiO_2—APTMS/FA system; computational details. This material is available free of charge *via* the Internet at http://pubs.acs.org.

REFERENCES AND NOTES

1. Bach, U.; Lupo, D.; Comte, P.; Moser, J. E.; Weissortel, F.; Salbeck, J.; Spreitzer, H.; Gratzel, M. Solid-State Dye-Sensitized Mesoporous TiO_2 Solar Cells with High Photon-to-Electron Conversion Efficiencies. *Nature (London, U. K.)* **1998**, *395*, 583–585.
2. Giepmans, B. N. G.; Adams, S. R.; Ellisman, M. H.; Tsien, R. Y. The Fluorescent Toolbox for Assessing Protein Location and Function. *Science* **2006**, *312*, 217–224.
3. Currie, M. J.; Mapel, J. K.; Heidel, T. D.; Goffri, S.; Baldo, M. A. High-Efficiency Organic Solar Concentrators for Photovoltaics. *Science* **2008**, *321*, 226–228.
4. Shi, X. G.; Wang, S. H.; Meshinchi, S.; Van Antwerp, M. E.; Bi, X. D.; Lee, I. H.; Baker, J. R Dendrimer-Entrapped Gold Nanoparticles as a Platform for Cancer-Cell Targeting and Imaging. *Small* **2007**, *3*, 1245–1252.
5. Medintz, I. L.; Clapp, A. R.; Goldman, E; Mattoussi, H. Quantum Dot Bioconjugates for Imaging, Labelling and Sensing. *Nat. Mater.* **2005**, *4*, 435–446.
6. Alivisatos, P. The Use of Nanocrystals in Biological Detection. *Nat. Biotechnol.* **2004**, *22*, 47–52.
7. Yu, S.; Choi, S.; Dickson, R. M. Shuttle-Based Fluorogenic Silver-Cluster Biolabels. *Angew. Chem., Int. Ed.* **2009**, *121*, 324–326.
8. Diebold, U. The Surface Science of Titanium Dioxide. *Surf. Sci. Rep.* **2003**, *48*, 53–229.
9. Gamble, L.; Henderson, M. A.; Campbell, C. T. Organofunctionalization of TiO_2(110): (3,3,3-Trifluoropropyl) Trimethoxysilane Adsorption. *J. Phys. Chem. B* **1998**, *102*, 4536–4543.
10. Gamble, L.; Hugenschmidt, M. B.; Campbell, C. T.; Jurgens, T. A.; Rogers, J. W. Adsorption and Reactions of Tetraethoxysilane (TEOS) on Clean and Water-Dosed Titanium Dioxide (110). *J. Am. Chem. Soc.* **1993**, *115*, 12096–12105.
11. Gamble, L.; Jung, L. S.; Campbell, C. T. Interaction of Silane Coupling Agents with the TiOs(110) Surface. *Langmuir* **1995**, *11*, 4505–4514.
12. Gamble, L.; Jung, L. S.; Campbell, C. T. Decomposition and Protonation of Surface Ethoxys on TiO_2(110). *Surf. Sci.* **1996**, *348*, 1–16.
13. Demirel, G.; Birlik, G.; Cakmak, M.; Caykara, T.; El-lialtioglu, S. An *ab Initio* Study of 3-Aminopropyltrimethoxysilane Molecule on Si(111)-($3^{1/2} \times 3^{1/2}$) Surface. *Surf. Sci.* **2007**, *601*, 3740–3744.
14. O'Regan, B.; Grätzel, M. A Low-Cost, High-Efficiency Solar Cell Based on Dye-Sensitized Colloidal TiO_2 Films. *Nature (London, U. K.)* **1991**, *353*, 737–739.
15. Yang, S.; Prendergast, D.; Neaton, J. B. Tuning Semiconductor Band Edge Energies for Solar Photocatalysis *via* Surface Ligand Passivation. *Nano Lett.* **2012**, *12*, 383–388.
16. Shalom, M.; Ruhle, S.; Hod, I.; Yahav, S.; Zaban, A. Energy Level Alignment in CdS Quantum Dot Sensitized Solar Cells Using Molecular Dipoles. *J. Am. Chem. Soc.* **2009**, *131*, 9876–9877.
17. Gaweda, S.; Stochel, G.; Szacilowski, K. Bioinspired Nanodevice Based on the Folic Acid/Titanium Dioxide System. *Asian J. Chem.* **2007**, *2*, 580–590.
18. Asahi, R.; Morikawa, T.; Ohwaki, T.; Aoki, K.; Taga, Y. Visible-Light Photocatalysis in Nitrogen-Doped Titanium Oxides. *Science* **2001**, *293*, 269–271.
19. Prokes, S. M.; Gole, J. L.; Chen, X. B.; Burda, C.; Carlos, W. E. Defect-Related Optical Behavior in Surface Modified TiO_2 Nanostructures. *Adv. Funct. Mater.* **2005**, *15*, 161–167.
20. Chen, X.; Mao, S. S. Titanium Dioxide Nanomaterials: Synthesis, Properties, Modifications, and Applications. *Chem. Rev.* **2007**, *107*, 2891–2959.
21. Di Valentin, C.; Pacchioni, G.; Selloni, A. Electronic Structure of Defect States in Hydroxylated and Reduced Rutile TiO_2(110) Surfaces. *Phys. Rev. Lett.* **2006**, *97*, 166803.
22. Pacchioni, G. Modeling Doped and Defective Oxides in Catalysis with Density Functional Theory Methods: Room for Improvements. *J. Chem. Phys.* **2008**, *128*, 182505.

23. Frisch, M. J.; Trucks, G. W.; Schlegel, H. B.; Scuseria, G. E.; Robb, M. A.; Cheeseman, J. R.; Montgomery, J. A., Jr., Vreven, T.; Kudin, K. N.; Burant, J. C. *et al*. *Gaussian 03;* Gaussian Inc: Wallingford, CT, 2004.
24. Becke, A. D. Density-Functional Exchange-Energy Approximation with Correct Asymptotic Behavior. *Phys. Rev. A* **1988**, *38*, 3098–3100.
25. Becke, A. D. Density-Functional Thermochemistry. III. The Role of Exact Exchange. *J. Chem. Phys.* **1993**, *98*, 5648–5652.
26. Lee, C. T.; Yang, W. T.; Parr, R. G. Development of the Colle−Salvetti Correlation-Energy Formula into a Functional of the Electron Density. *Phys. Rev. B* **1988**, *37*, 785–789.
27. Mastropaolo, D.; Camerman, A.; Camerman, N. Folic Acid: Crystal Structure and Implications for Enzyme Binding. *Science* **1980**, *210*, 334–336.
28. Wakabayashi, K.; Yamaguchi, Y.; Sekiya, T.; Kurita, S. Time-Resolved Luminescence Spectra in Colorless Anatase TiO_2 Single Crystal. *J. Lumin.* **2005**, *112*, 50–53.
29. Liu, W. T. Nanoparticles and Their Biological and Environmental Applications. *J. Biosci. Bioeng.* **2006**, *102*, 1–7.
30. Cheng, H. Z.; Selloni, A. Surface and Subsurface Oxygen Vacancies in Anatase TiO_2 and Differences with Rutile. *Phys. Rev. B: Condens. Matter Mater. Phys.* **2009**, *79*, 092101.
31. Morgan, B. J.; Watson, G. W. A DFT + U Description of Oxygen Vacancies at the TiO_2 Rutile (110) Surface. *Surf. Sci.* **2007**, *601*, 5034–5041.
32. Bradsen, B. H.; Joachain, C. J. *Physics of Atoms and Molecules*; Longman: London, 1983.
33. Thomas, A. H.; Lorente, C.; Capparelli, A. L.; Pokhrel, M. R.; Braun, A. M.; Oliveros, E. Fluorescence of Pterin, 6-Formylpterin, 6-Carboxypterin and Folic Acid in Aqueous Solution: pH Effects. *Photochem. Photobiol. Sci.* **2002**, *1*, 421–426.
34. Schäfer, W.; Wegener, M. *Semiconductor Optics and Transport Phenomena*; Springer, New York, 2002.
35. Weinberg, Z. A.; Rubloff, G. W.; Bassous, E. Transmission, Photoconductivity, and the Experimental Band Gap of Thermally Grown SiO_2 Films. *Phys. Rev. B* **1979**, *19*, 3107–3117.
36. Saha, N. C.; Tompkins, H. G. Titanium Nitride Oxidation Chemistry: An X-ray Photoelectron Spectroscopy Study. *J. Appl. Phys.* **1992**, *72*, 3072–3079.
37. Skuja, L. N.; Silin, A. R. Optical Properties and Energetic Structure of Non-Bridging Oxygen Centers in Vitreous SiO_2. *Phys. Status Solidi A* **1979**, *56*, K11–K13.